PHYSICS

Demonstration of slow light in rubidium vapor using single photons from a trapped ion

J. D. Siverns[1], J. Hannegan[1], Q. Quraishi[1,2]*

Practical implementation of quantum networks is likely to interface different types of quantum systems. Photonically linked hybrid systems, combining unique properties of each constituent system, have typically required sources with the same photon emission wavelength. Trapped ions and neutral atoms both have compelling properties as nodes and memories in a quantum network but have never been photonically linked because of vastly different operating wavelengths. Here, we demonstrate the first interaction between neutral atoms and photons emitted from a single trapped ion. We use slow light in ^{87}Rb vapor to delay photons originating from a trapped ^{138}Ba$^+$ ion by up to 13.5 ± 0.5 ns, using quantum frequency conversion to overcome the frequency difference between the ion and neutral atoms. The delay is tunable and preserves the temporal profile of the photons. This result showcases a hybrid photonic interface usable as a synchronization tool—a critical component in any future large-scale quantum network.

INTRODUCTION

Establishing scalable quantum networks requires integration of disparate quantum components. Photonic linking of quantum systems to form hybrid platforms has been shown using single atoms (*1*, *2*), Bose-Einstein condensates (*2*), solid-state systems (*3*), atomic vapors (*4*), and atomic ensembles (*5*). This progress in hybrid networking has typically focused on the special case in which the native photon wavelength of each system is the same, either by definition or through direct engineering of one of the photon sources itself (*3*). Such a strict requirement will likely not be achievable in a practical network, especially as photons emitted from current devices used in quantum communication technologies span a wide portion of the photonic spectrum. To overcome this spectral mismatch, quantum frequency conversion (QFC) can be used to convert a photon's frequency to another frequency while preserving its quantum properties (*6–10*). This approach allows for different types of quantum systems to be connected and is, therefore, more universally applicable than prior methods. A hybrid system that combines highly desirable features of different components, such as high-fidelity trapped ion nodes with robust neutral atom quantum storage, would realize a viable quantum networking tool.

Trapped ions are strong candidates for communication nodes owing to their long qubit lifetime (*11*) and high-fidelity ion-photon entanglement (*12*), while neutral atoms are versatile quantum systems, useful as memories (*13–16*), photon storage media (*17*), or for tunable photon delay via slow light. Considerable investment in design, control, and development of trapped ion and neutral atom quantum technologies has yielded remarkable progress in quantum networking (*18–20*), computing (*21*, *22*), metrology (*23–25*), and simulation (*26–30*). Neutral atom vapors and magneto-optically trapped atoms are commonly used as slow-light media (*31–33*) either for pulses of light or, as in this work, for single photons. Tunable photonic delays, possible via slow light, would be useful for photon synchronization when implementing networking protocols via photonic interference (*13*). In this work, we show the first interaction between neutral atoms and photons emitted by an ion by slowing photons generated from a single trapped ion in a neutral atom vapor.

RESULTS

Slow light in an atomic vapor using two absorption resonances

Slow light in atomic vapors requires a medium that has a low group velocity and can be achieved using photons with a frequency between two absorption resonances of a medium (*33*). The two absorption resonances may be interrogated via electromagnetically induced transparency (EIT) or far-off resonance, as shown in Fig. 1A. In this work, we use the two D$_2$ absorption resonances (*31*, *32*) created by the hyperfine ground state splitting in ^{87}Rb. This method requires a less complex experimental setup as compared with the EIT methods because only single photons at the correct frequency are required to achieve slowing with no additional lasers required. For our case, the complex index of refraction is given by

$$n(\delta) = 1 - A\left(\frac{g_1}{\delta + \Delta_+ + i\gamma/2} + \frac{g_2}{\delta - \Delta_- + i\gamma/2}\right) \quad (1)$$

where g_1 and g_2 are the relative strengths of the two resonances (7/16 and 9/16, respectively, for ^{87}Rb), γ is the homogeneous linewidth, δ is the detuning from peak transmission, and $\Delta_\pm = \omega_s \pm \Delta$ with $\omega_s = (\omega_2 - \omega_1)/2$ and $\Delta = \omega_s((g_1^{1/3} - g_2^{1/3})/(g_1^{1/3} + g_2^{1/3}))$. The frequencies of the two absorption peaks are given as ω_1 and ω_2. The total strength of the resonance, A, in a vapor cell is a function of the atomic number density, N, and is given by

$$A = \frac{N|\mu|^2}{2\varepsilon_0 \hbar(g_1 + g_2)} \quad (2)$$

where μ is the effective far-detuned dipole moment, ε_0 is the vacuum permittivity, and $\hbar$ is the reduced Plank constant. Using the real part of Eq. 1, $n_r(\delta)$ (Fig. 1B), it is possible to derive the group velocity

$$v_g(\delta) = \left(\frac{\omega_0}{c}\frac{dn_r(\delta)}{d\omega}\right)^{-1} \quad (3)$$

where c is the speed of light in vacuum and ω_0 is the optical frequency from the midpoint between the two absorption resonances to the excited P$_{3/2}$ level and, in this work, the frequency of the photons emitted from the Ba$^+$ ion after QFC. When the photon's optical frequency is
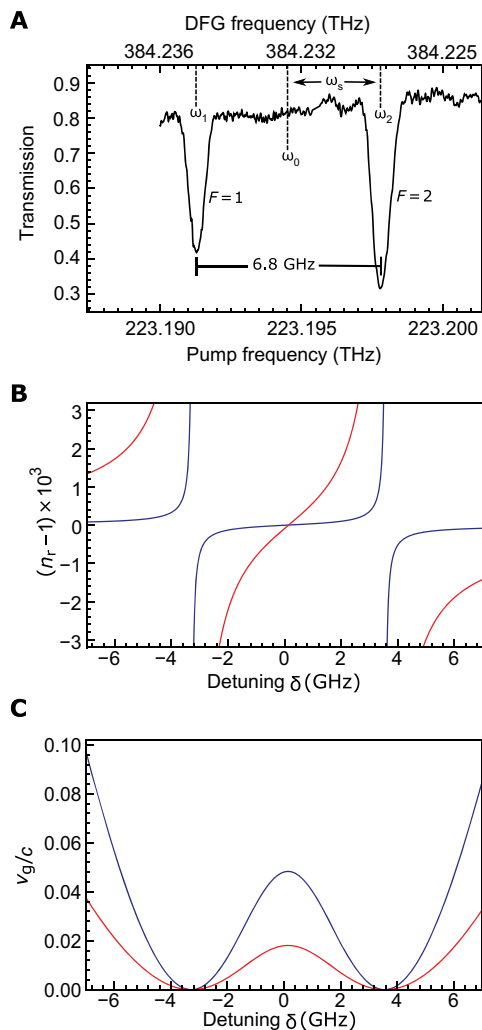
[1]Joint Quantum Institute, IREAP, and Department of Physics, University of Maryland College Park, MD 20742, USA. [2]Army Research Laboratory, Adelphi, MD 20783, USA.
*Corresponding author. Email: quraishi@umd.edu

Fig. 1. Absorption, refractive index, and group velocity within a warm ^{87}Rb vapor. (**A**) Absorption profile of the ^{87}Rb D_2 line using 780 nm obtained via QFC from a 493-nm laser light with the cell at room temperature. The pump laser's mode-hop-free tuning range limits the frequency tuning range. The refractive index (**B**) and group velocity (**C**) in the vicinity of the two absorption peaks as a function of detuning from peak transmission, δ, at 373 K (blue) and 423 K (red). DFG, difference frequency generation.

pump laser, with frequency ω_{pump} near 1343 nm, and both are free space coupled into a periodically poled lithium niobate (PPLN) waveguide where difference frequency generation (DFG) occurs via a $\chi^{(2)}$ nonlinearity. The DFG process results in photons produced at $\omega_0 = \omega_{ion} - \omega_{pump}$ (see Materials and Methods for details) (35, 36). After appropriate frequency tuning of the pump laser, we can produce 780-nm photons (7) with a frequency that is between the two optical absorption resonances of the ^{87}Rb D_2 line, ω_0 in Fig. 1A, for implementing slow light. The conversion efficiency of the PPLN device is a function of the pump power coupled into the waveguide (37). However, while operating at the maximum conversion efficiency increases the number of 780-nm photons produced, the larger pump power increases the number of anti-Stokes noise photons (7). It is, therefore, critical to maximize the signal-to-noise ratio (SNR) of the converted light rather than the total amount of converted light, as shown in Fig. 3. We convert the 493-nm photons using DFG with pump light near 1343 nm to generate 780 nm, as described in (7), and tune the 780-nm optical frequency by tuning the pump optical frequency. The output of the PPLN is butt coupled to an 800-nm single-mode fiber to capture 780-nm photons and to spatially filter out other modes including the PPLN input modes.

Once filtered (see Materials and Methods for details), the photons are sent through a 75-mm-long heated glass cell filled with enriched ^{87}Rb (Triad Technology, TT-RB87-25X-75-P-CAL2O3) and then detected on an avalanche photodiode (APD) (PerkinElmer, SPCM-AQR-15). The inside of the cell is coated with aluminum oxide to reduce rubidium diffusion into the glass when the cell is at elevated temperatures. Passing photons through the rubidium cell at room temperature causes absorption and scattering of some of the photons, which decreases the SNR to ≈ 6. To measure the temporal shape, we recorded the arrival time of the photons at the APD with respect to the 650-nm excitation acousto-optic modulator (AOM) transistor-transistor logic (TTL) pulse (see Materials and Methods and Fig. 2A for details) using a time-correlated single-photon counter (TCSPC) with a resolution of 512 ps (PicoQuant, PicoHarp 300). Figure 2D shows the area-normalized temporal shape histograms of photons emitted directly from the Ba$^+$ ion at 493 nm and of photons' frequency converted to a frequency halfway between the two D_2 absorption resonances and passed through the ^{87}Rb vapor cell at room temperature. These histograms clearly show the preservation of the temporal shape even after QFC and traversal through the cell at room temperature.

Slowing of photons from the trapped ion in Rb vapor
By increasing the temperature of the vapor cell, the density of rubidium atoms, N, may be increased, leading to a larger change of refractive index and a lower group velocity, as described by Eqs. 1 and 3 and shown in Fig. 1B and Fig. 1C, respectively. The cell was heated to temperatures ranging from 296 K (room temperature) to 395 K to demonstrate tunable single-photon delays of up to 13.5 ± 0.5 ns (Figs. 4 and 5). The temperature of the Rb cell is measured on a cold finger protruding from the cell. The temperature of this cold finger (the coldest part of the cell) controls the density of atoms in the cell. This is the reported temperature in Figs. 4 and 5. Because of an increase in absorption as the atomic density of the vapor cell increases combined with reduced alignment efficiency at higher temperatures in our setup, the SNR monotonically falls with temperature and approaches ≈ 1 at 395 K. Although there is a lower SNR value for the higher temperature settings, the photon delays are still clearly visible, and the pulse retains
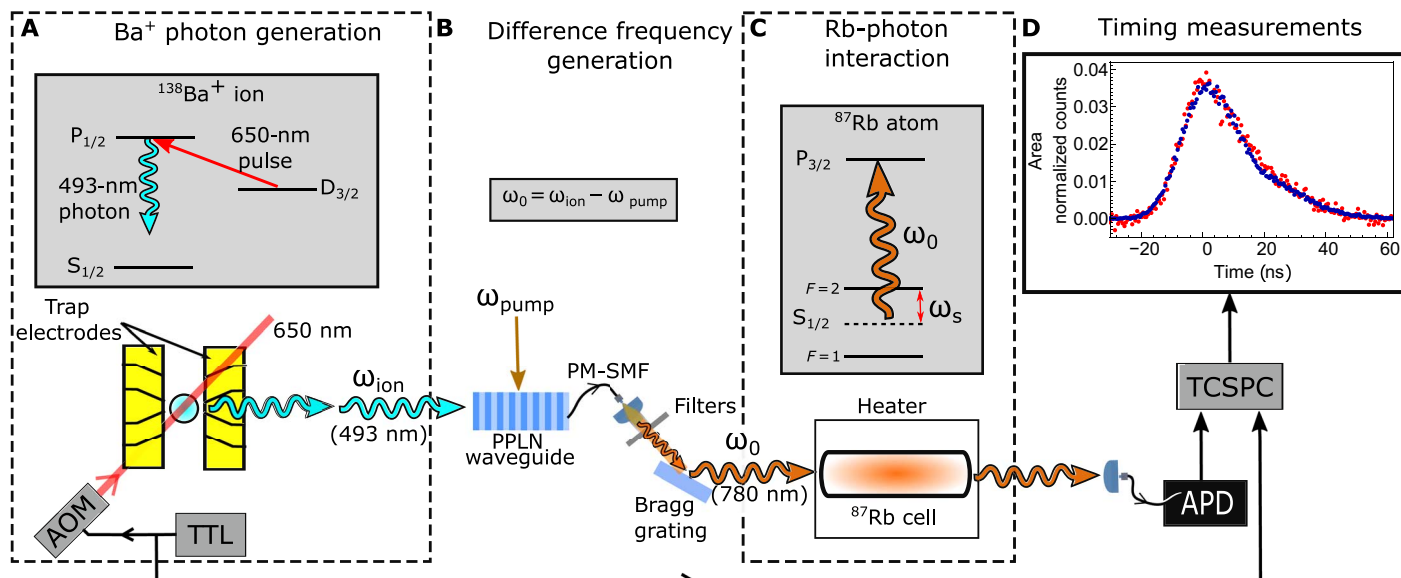
tuned to ω_0, there is a maximum in transmission (Fig. 1A). From Eq. 3, in the normal dispersion regime, one can see that a photon with a frequency at the midpoint of two absorption resonances ($\delta = 0$) will have a greatly reduced group velocity (Fig. 1C). It is also clear that if N in Eq. 2 is increased, the group velocity will be reduced. Therefore, by changing the atomic number density, N, it is possible to tune the photon delay.

QFC from 493 to 780 nm and transmission through a room temperature Rb cell
The source of the 493-nm single photons is a ^{138}Ba$^+$ ion (see Materials and Methods for details), trapped using voltages applied to segmented blades housed in an ultrahigh vacuum chamber (Fig. 2A) (34, 35). These photons are collected by a 0.4 NA (numerical aperture) lens, then fiber coupled, and, lastly, sent to the QFC setup (Fig. 2B). Here, the photons emitted by the ion, with frequency ω_{ion}, are combined with a

Fig. 2. Experimental schematic of photon production from a ^{138}Ba$^+$ ion, QFC, and photonic slowing in a warm neutral ^{87}Rb vapor. (**A**) The energy levels of ^{138}Ba$^+$ and schematic showing the ion confined in a segmented blade trap. A TTL pulse-activated AOM controls a 650-nm excitation light. (**B**) The QFC setup including a PPLN waveguide. Converted light, ω_0, is at the difference frequency between photons emitted from the ion at ω_{ion} and pump photons at ω_{pump}. The output of the PPLN is fiber coupled to a polarization maintaining single-mode fiber (PM-SMF). A series of filters and a Bragg grating filter out pump light and unconverted 493-nm light, which reduces the amount of anti-Stokes noise. (**C**) A ^{87}Rb energy level diagram and a vapor cell housed inside a heater through which converted single photons pass. (**D**) Photons are detected on an APD, and a TCSPC collects the arrival time of the photons with respect to the TTL sent to the AOM. As an example, single-photon temporal shapes at 493 nm (blue circles) and frequency-converted photons after passing through the cell at room temperature (red circles) are shown.
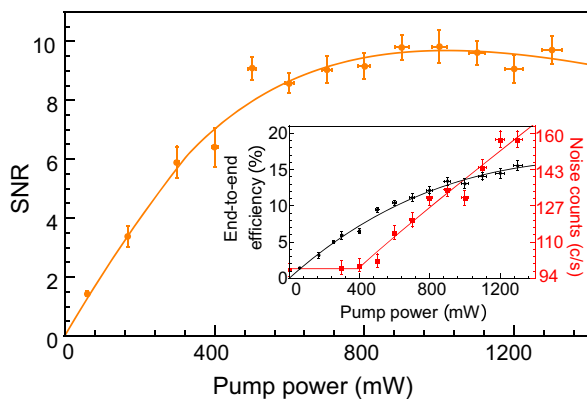

Fig. 3. SNR measured after filtering of the frequency-converted ion signal. The orange curve is the SNR given the measured conversion efficiencies and noise at each pump power. Inset: Measured conversion efficiency (black) and measured noise counts (red) on the APD as a function of pump power. The black curve is a theoretical fit to the efficiency data, and the red curve is an empirical fit to the noise.

its initial temporal profile, as shown in Fig. 5 (inset). In Fig. 5, we plot the photon delay as a function of cell temperature and observe good agreement with the theory curve derived from Eq. 3, with a scaling to fit the atomic number density, N.

The photon delay was determined by temporally shifting each delayed photon to overlap with a room temperature photon shape. The photons emitted by the Ba$^+$ ion (with a linewidth $\approx 2\pi \times 15$ MHz) and the drift of the pump laser (≈ 10 MHz) put an upper limit on the optical frequency stability of the converted photons. The converted
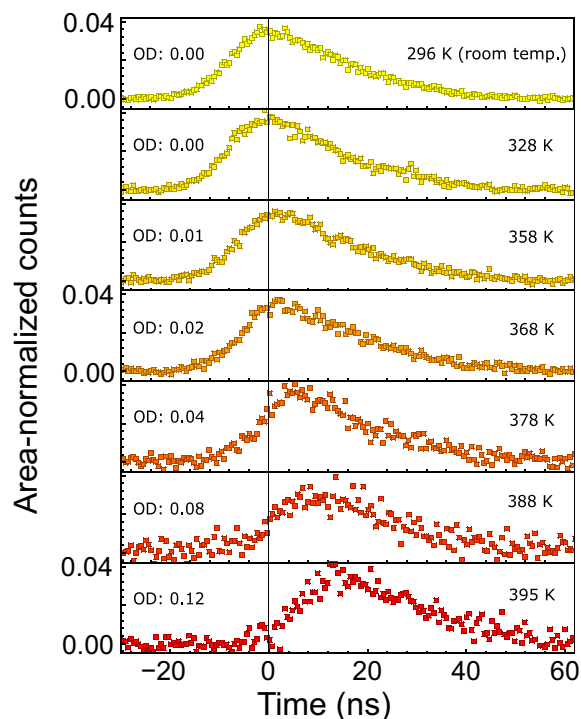

Fig. 4. Area-normalized temporal photon shapes. Area-normalized temporal shapes of frequency-converted photons that have passed through a warm ^{87}Rb vapor cell. The ^{87}Rb vapor cell temperature is set to the values indicated. The optical density (OD) of the warm vapor is stated for each temperature, at a frequency ω_0, and using the same atomic density, N, used to fit the delay curve in Fig. 5.
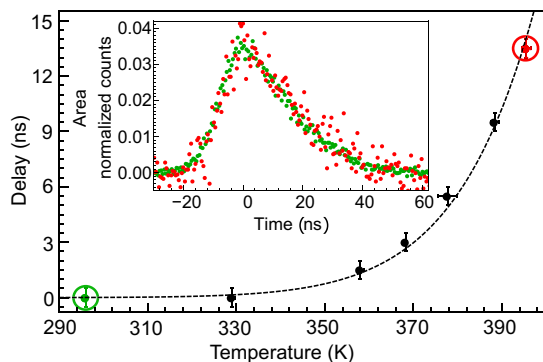
Fig. 5. Delay of the frequency-converted photons emitted from the trapped Ba$^+$ ion after passing through a ^{87}Rb vapor cell as a function of the cell's temperature. The dashed theory curve is a scaled version of Eq. 3 to account for N. The temperature and delay error bars are due to temperature fluctuations over the course of the experiment and the bin width of the histogram photon arrival time data, respectively. Inset: Overlap of temporal shapes of photons transmitted through a 296-K room temperature cell (green circles) and a 395-K cell (red circles). The relative delay between the two traces has been removed to allow for comparison.

photon's linewidth is orders of magnitude narrower than the splitting between the ^{87}Rb D$_2$ absorption peaks ($\approx$ 6.8 GHz), so there is a negligible change in the group velocity (slope of Fig. 1C) between subsequent slowed photons. In this case, even considering the upper limit of frequency drift, there is negligible fractional broadening of the photon's temporal width. This is in contrast to previous work using quantum dots where the emitted photon linewidths are similar to the splitting of the ^{87}Rb D$_2$ absorption lines, resulting in large broadening of the delayed photons (3). The inset of Fig. 5 shows the temporal shape of a single photon passed through the vapor cell at room temperature (green circles) and at 395 K (red circles). Although the delay is only $\approx$ 0.5 times the temporal width of the photons produced by the Ba$^+$ ion in this experiment, additional delays (32, 38) and improved transmission are possible by increasing the nonlinear refractive index in the vapor by extending this work using methods such as EIT (17).

DISCUSSION

In summary, we have demonstrated the first interaction of photons emitted from a trapped ion with a neutral atom system by slowing frequency-converted photons emitted from a trapped ion in a warm rubidium vapor cell. Tunable delays of up to 13.5 ± 0.5 ns were observed with negligible temporal dispersion of the photons, making this system ideal for use as a device for tunable synchronization of remote quantum nodes in a hybrid quantum network. This approach offers a path toward photonic quantum gates between remotely situated ions and neutral atoms, especially given that these two systems can emit photons of comparable temporal profile. In addition, this work paves the way for future quantum-state transfer between ions and neutral atoms, experiments such as ion–neutral atom photonic entanglement distribution, and photonic storage of flying qubits emitted from trapped ions using existing highly developed neutral atom technologies.

MATERIALS AND METHODS
Filtering of the converted 780-nm photons
The frequency-converted 780-nm photons were passed through four free-space optical interference filters to remove pump light and un-
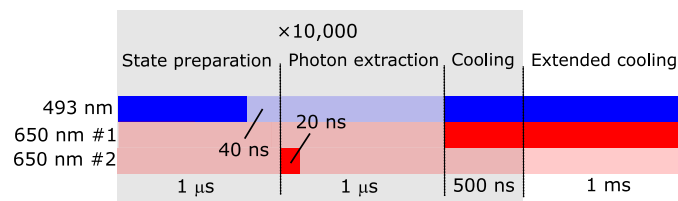

Fig. 6. Experimental pulse sequence. The experimental pulse sequence showing the timing of the laser beams used to state prepare, extract a single photon, and Doppler cool the ion. The parts of the sequence contained in the gray shading are repeated 10,000 times before an extended cooling cycle is performed.

converted 493-nm photons (two each of Semrock: LL01-780-25 and FF01-1326/SP-25). With these filters in place, no detectable pump or 493-nm photon counts above the APD dark noise were measured at the pump powers used in this work. In addition, a Bragg grating with a spectral bandwidth of 0.15 nm and $\approx$ 90% efficiency was used to filter anti-Stokes noise created by the high-intensity pump light (7). With this filtering approach, it is possible to achieve the SNR numbers, as shown in Fig. 3, and we operated with around 800-mW pump power. The inset shows both the end-to-end efficiency (defined as the percentage of 493-nm photons entering the QFC setup that are converted to 780 nm) and the noise counts produced as a function of pump power. The maximum achieved SNR and end-to-end efficiency of the conversion were measured to be 9.8 ± 0.6% and 15.5 ± 0.7%, respectively. Using these numbers and including the 0.4 NA collection lens (4% collection) and fiber coupling of the 493-nm photons ($\approx$ 35%), on average $\approx$ 2.4 in every 1000 photons at 493 nm produced by the ion were converted to 780-nm photons. The addition of the narrowbandwidth (0.15 nm) Bragg grating has allowed an increase in SNR of around a factor of five from previously reported work (7). When laser light at 493 nm is converted, we were able to obtain the Rb absorption curve shown in Fig. 1A.

Pulse sequence for generation of single photons from ^{138}Ba$^+$
To produce single 493-nm photons, the pulse sequence shown in Fig. 6 was used. First, the ion was prepared in the long-lived D$_{3/2}$ level using the 493-nm light incident on the ion for $\approx$ 1 μs. The ion was then excited into the P$_{1/2}$ level using the 650-nm light pulsed on for $\approx$ 20 ns using a TTL-controlled AOM (IntraAction, ATM 80-A1). Once in the P$_{1/2}$ level, the ion decays into either the S$_{1/2}$ state (with $\approx$ 75% probability) or back into the D$_{3/2}$ state (with $\approx$ 25% probability). If the former occurs, then a 493-nm photon was emitted and collected using a 0.4 NA lens (4% collection efficiency) and coupled into a short (a few meters) single-mode fiber ($\approx$ 35% coupling). Otherwise, a 650-nm photon was emitted and not detected. After a delay of 980 ns, a short 500-ns cycle of Doppler cooling was performed before the ion was re-initialized in the D$_{3/2}$ state. This process was repeated 10,000 times before both cooling lasers were turned on to Doppler cool the ion for 1 ms to prevent excessive heating of the ion. Between preparation and extraction pulses, all beams were turned off for 40 ns to prevent accidental detection of 493-nm light originating from the preparation beam rather than the ion. All the optical beams used to interrogate the ion consist of all polarizations. This scheme ensures only one 493-nm photon is emitted in the measurement window, as once this photon is emitted, the ion remains in the ground state with no excitation field present. This scheme is also easily adaptable to produce ion-photon entanglement (35).

REFERENCES AND NOTES

1. H. M. Meyer, R. Stockill, M. Steiner, C. Le Gall, C. Matthiesen, E. Clarke, A. Ludwig, J. Reichel, M. Atatüre, M. Köhl, Direct photonic coupling of a semiconductor quantum dot and a trapped ion. *Phys. Rev. Lett.* **114**, 123001 (2015).

2. M. Lettner, M. Mücke, S. Riedl, C. Vo, C. Hahn, S. Baur, J. Bochmann, S. Ritter, S. Dürr, G. Rempe, Remote entanglement between a single atom and a Bose-Einstein condensate. *Phys. Rev. Lett.* **106**, 210503 (2011).

3. N. Akopian, L. Wang, A. Rastelli, O. G. Schmidt, V. Zwiller, Hybrid semiconductor-atomic interface: Slowing down single photons from a quantum dot. *Nat. Photonics* **5**, 230–233 (2011).

4. P. Siyushev, G. Stein, J. Wrachtrup, I. Gerhardt, Molecular photons interfaced with alkali atoms. *Nature* **509**, 66–70 (2014).

5. H. Zhang, X.-M. Jin, J. Yang, H.-N. Dai, S.-J. Yang, T.-M. Zhao, J. Rui, Y. He, X. Jiang, F. Yang, G.-S. Pan, Z.-S. Yuan, Y. Deng, Z.-B. Chen, X.-H. Bao, S. Chen, B. Zhao, J.-W. Pan, Preparation and storage of frequency-uncorrelated entangled photons from cavity-enhanced spontaneous parametric downconversion. *Nat. Photonics* **5**, 628–632 (2011).

6. N. Maring, P. Farrera, K. Kutluer, M. Mazzera, G. Heinze, H. de Riedmatten, Photonic quantum state transfer between a cold atomic gas and a crystal. *Nature* **551**, 485–488 (2017).

7. J. D. Siverns, J. Hannegan, Q. Quraishi, Neutral-atom wavelength- compatible 780 nm single photons from a trapped ion via quantum frequency conversion. *Phys. Rev. Appl.* **11**, 014044 (2019).

8. M. Bock, P. Eich, S. Kucera, M. Kreis, A. Lenhard, C. Becher, J. Eschner, High-fidelity entanglement between a trapped ion and a tele- com photon via quantum frequency conversion. *Nat. Commun.* **9**, 1998 (2018).

9. T. Walker, K. Miyanishi, R. Ikuta, H. Takahashi, S. Vartabi Kashanian, Y. Tsujimoto, K. Hayasaka, T. Yamamoto, N. Imoto, M. Keller, Long-distance single photon transmission from a trapped ion via quantum frequency conversion. *Phys. Rev. Lett.* **120**, 203601 (2018).

10. R. Ikuta, T. Kobayashi, T. Kawakami, S. Miki, M. Yabuno, T. Yamashita, H. Terai, M. Koashi, T. Mukai, T. Yamamoto, Polarization insensitive frequency conversion for an atom-photon entanglement distribution via a telecom network. *Nat. Commun.* **9**, 1997 (2018).

11. C. Langer, R. Ozeri, J. D. Jost, J. Chiaverini, B. Demarco, A. Ben-Kish, R. B. Blakestad, J. Britton, D. B. Hume, W. M. Itano, D. Leibfried, R. Reichle, T. Rosenband, T. Schaetz, P. O. Schmidt, D. J. Wineland, Long-lived qubit memory using atomic ions. *Phys. Rev. Lett.* **95**, 060502 (2005).

12. A. Stute, B. Casabone, P. Schindler, T. Monz, P. O. Schmidt, B. Brandstätter, T. E. Northup, R. Blatt, Tunable ion–photon entanglement in an optical cavity. *Nature* **485**, 482–485 (2012).

13. L.-M. Duan, M. D. Lukin, J. I. Cirac, P. Zoller, Long-distance quantum communication with atomic ensembles and linear optics. *Nature* **414**, 413–418 (2001).

14. B. Jing, X.-J. Wang, Y. Yu, P.-F. Sun, Y. Jiang, S.-J. Yang, W.-H. Jiang, X.-Y. Luo, J. Zhang, X. Jiang, X.-H. Bao, J.-W. Pan, Entanglement of three quantum memories via interference of three single photons. *Nat. Photonics* **13**, 210–213 (2019).

15. H. P. Specht, C. Nölleke, A. Reiserer, M. Uphoff, E. Figueroa, S. Ritter, G. Rempe, A single-atom quantum memory. *Nature* **473**, 190–193 (2011).

16. R. Finkelstein, E. Poem, O. Michel, O. Lahad, O. Firstenberg, Fast, noise- free memory for photon synchronization at room temperature. *Sci. Adv.* **4**, eaap8598 (2018).

17. O. Katz, O. Firstenberg, Light storage for one second in room-temperature alkali vapor. *Nat. Commun.* **9**, 2074 (2018).

18. D. Hucul, I. V. Inlek, G. Vittorini, C. Crocker, S. Debnath, S. M. Clark, C. Monroe, Modular entanglement of atomic qubits using photons and phonons. *Nat. Phys.* **11**, 37–42 (2015).

19. H. J. Kimble, The quantum internet. *Nature* **453**, 1023–1030 (2008).

20. A. Kuhn, M. Hennrich, G. Rempe, Deterministic single-photon source for distributed quantum networking. *Phys. Rev. Lett.* **89**, 067901 (2002).

21. C. Figgatt, D. Maslov, K. A. Landsman, N. M. Linke, S. Debnath, C. Monroe, Complete 3-qubit grover search on a programmable quantum computer. *Nat. Commun.* **8**, 1918 (2017).

22. H. Häffner, C. F. Roos, R. Blatt, Quantum computing with trapped ions. *Phys. Rep.* **469**, 155–203 (2008).

23. J.-S. Chen, S. M. Brewer, C. W. Chou, D. J. Wineland, D. R. Leibrandt, D. B. Hume, Sympathetic ground state cooling and time-dilation shifts in an $^{27}Al^+$ optical clock. *Phys. Rev. Lett.* **118**, 053002 (2017).

24. S. L. Campbell, R. B. Hutson, G. E. Marti, A. Goban, N. Darkwah Oppong, R. L. McNally, L. Sonderhouse, J. M. Robinson, W. Zhang, B. J. Bloom, J. Ye, A Fermi-degenerate three-dimensional optical lattice clock. *Science* **358**, 90–94 (2017).

25. T. Rosenband, D. B. Hume, P. O. Schmidt, C. W. Chou, A. Brusch, L. Lorini, W. H. Oskay, R. E. Drullinger, T. M. Fortier, J. E. Stalnaker, S. A. Diddams, W. C. Swann, N. R. Newbury, W. M. Itano, D. J. Wineland, J. C. Bergquist, Frequency ratio of Al$^+$ and Hg$^+$ single-ion optical clocks; metrology at the 17th decimal place. *Science* **319**, 1808–1812 (2008).

26. R. Blatt, C. F. Roos, Quantum simulations with trapped ions. *Nat. Phys.* **8**, 277–284 (2012).

27. I. Bloch, J. Dalibard, S. Nascimbene, Quantum simulations with ultracold quantum gases. *Nat. Phys.* **8**, 267–276 (2012).

28. R. Islam, C. Senko, W. C. Campbell, S. Korenblit, J. Smith, A. Lee, E. E. Edwards, C. C. Wang, J. K. Freericks, C. Monroe, Emergence and frustration of magnetism with variable-range interactions in a quantum simulator. *Science* **340**, 583–587 (2013).

29. J. Zhang, G. Pagano, P. W. Hess, A. Kyprianidis, P. Becker, H. Kaplan, A. V. Gorshkov, Z. X. Gong, C. Monroe, Observation of a many-body dynamical phase transition with a 53-qubit quantum simulator. *Nature* **551**, 601–604 (2017).

30. H. Bernien, S. Schwartz, A. Keesling, H. Levine, A. Omran, H. Pichler, S. Choi, A. S. Zibrov, M. Endres, M. Greiner, V. Vuletić, M. D. Lukin, Probing many-body dynamics on a 51-atom quantum simulator. *Nature* **551**, 579–584 (2017).

31. R. M. Camacho, M. V. Pack, J. C. Howell, Low-distortion slow light using two absorption resonances. *Phys. Rev. A* **73**, 063812 (2006).

32. R. M. Camacho, M. V. Pack, J. C. Howell, A. Schweinsberg, R. W. Boyd, Wide-bandwidth, tunable, multiple-pulse-width optical delays using slow light in cesium vapor. *Phys. Rev. Lett.* **98**, 153601 (2007).

33. J. B. Khurgin, Slow light in various media: A tutorial. *Adv. Opt.Photonics* **2**, 287–318 (2010).

34. J. D. Siverns, Q. Quraishi, Ion trap architectures and new directions. *Quantum Inf. Process.* **16**, 314 (2017).

35. J. D. Siverns, X. Li, Q. Quraishi, Ion–photon entanglement and quantum frequency conversion with trapped Ba$^+$ ions. *Appl. Optics* **56**, B222–B230 (2017).

36. P. Kumar, Quantum frequency conversion. *Opt. Lett.* **15**, 1476–1478 (1990).

37. J. S. Pelc, L. Ma, C. R. Phillips, Q. Zhang, C. Langrock, O. Slattery, X. Tang, M. M. Fejer, Long-wavelength-pumped upconversion single-photon detector at 1550 nm: Performance and noise analysis. *Opt. Express* **19**, 21445–21456 (2011).

38. O. Kocharovskaya, Y. Rostovtsev, M. O. Scully, Stopping light via hot atoms. *Phys. Rev. Lett.* **86**, 628–631 (2001).